

Anomalous Ion Confinement Penalties and Giant Ion-Screening Effects in One-Dimensional Nanopores

Kevin Leung*

*Sandia National Laboratories, Albuquerque,
New Mexico 87185, USA; kleung@sandia.gov*

(Dated: March 16, 2026)

Abstract

Nanoconfinement reduces the favorable hydration free energies of single ions, and is correlated with ion rejection and modified chemical reactivity in water-filled nanopores. Many factors contribute to the magnitude of the observed confinement effect. Here we use simple classical force fields and non-polarizable carbon nanotubes filled with water as minimal, “hydrogen atom”-like models to evaluate the single-ion intrinsic confinement hydration free energy penalty ($\Delta\Delta G_{\text{hyd}}$). In tubes of radius $R=7.5$ Å, we predict $\Delta\Delta G_{\text{hyd}}$'s that are up to 7.8 kcal/mol, are much larger for Cl^- than the smaller Na^+ ion, and contradict the canonical Born Equation for ion solvation. Adding a 1.0 M background electrolyte reduces $\Delta\Delta G_{\text{hyd}}$ for the Na^+/Cl^- pair by an amount exceeding the Debye-Hückel estimate in unconfined media by almost an order of magnitude. We identify concentration-dependent ion-screening of confinement effects as a major, unheralded consequence of electrolytes in cylindrical nanopores.

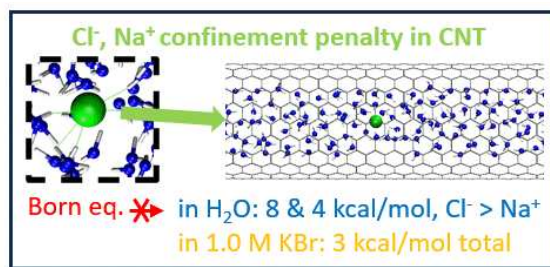


FIG. 0: TOC Graphic.

It is widely accepted that the hydration free energies of single ions (ΔG_{hyd}) become less negative/favorable in confined liquid media.¹⁻³ A confinement free energy penalty ($\Delta\Delta G_{\text{hyd}}$, or ΔG_{hyd} referenced to unconfined systems) is qualitatively consistent with observed ion-rejection from porous membranes,⁴ increased ion-pairing,⁵ and modified surface adsorption⁶ and chemical reactivity,^{3,7-13} which are phenomena relevant to ion separation, extraction, desalination of water, and energy applications.¹⁴⁻²⁰

A heuristic rationale for $\Delta\Delta G_{\text{hyd}}$ is given by the canonical, widely-cited Born Equation for ion solvation:²¹

$$\Delta G_{\text{hyd};\text{B}} = -(q^2/2a_{\text{eff}})(1 - 1/\epsilon); \text{ therefore} \quad (1)$$

$$\Delta\Delta G_{\text{hyd};\text{B}} = (q^2/2a_{\text{eff}})(1/\epsilon - 1/\epsilon_w), \quad (2)$$

where q is the ionic charge, a_{eff} is the effective ionic radius, ϵ_w and ϵ are the effective dielectric constants of the unconfined reference and confined systems, respectively, and atomic units are used. If the relevant ϵ under confinement is less than ϵ_w , as has been widely accepted,²²⁻³³ $\Delta\Delta G_{\text{hyd}} > 0$, and the ion tends to be rejected from confined spaces. Since cations and anions are present in any electrolyte, elucidating which ion is most unfavorable will significantly impact nanoscale applications. But many factors (Fig. 1) are left out of Eqs. 1-2. (1) The dielectric (ϵ) response under confinement is anisotropic,²⁴⁻³³ and ϵ -calculations via molecular dynamics (MD) simulations in nano-cylinders are challenging even at the conceptual level.³³ (2) Every interface in the system, e.g., that arising from a water reservoir (Fig. 1b),³⁴⁻³⁶ yields an additive contribution to $\Delta\Delta G_{\text{hyd}}$. This ‘‘interface (or surface) potential’’ contribution already exists for unconfined water in contact with the vapor phase³⁷ and does not decay with distance from the interface.^{37,38} (3) Dielectric screening of the single ion by the reservoir (which exists in many MD models³⁶) reduces $\Delta\Delta G_{\text{hyd}}$. Models used in such MD studies (e.g., Refs. 34,36) tend to have pore lengths which are too short, and water reservoirs too close to the confined ion, compared to real-life, micron-long nanopores. (4) The convergence of $\Delta\Delta G_{\text{hyd}}$ with system sizes has not been systematically explored (e.g., with respect to L_1 , L_2 , and L_z in Fig. 1b). These factors make MD-based interpretation of confinement effects challenging.^{9,36}

In this work, we focus on one-dimensional pores. Many naturally-occurring and synthetic nanopores are cylindrical and microns in lengths, like silica-based MCM-41, SBA-15 widely studied for nanoscience applications,⁹ geochemically relevant imogolites,³⁹ and carbon nanotubes (CNT). The water-induced ‘‘intrinsic confinement’’ contribution to $\Delta\Delta G_{\text{hyd}}$ in the

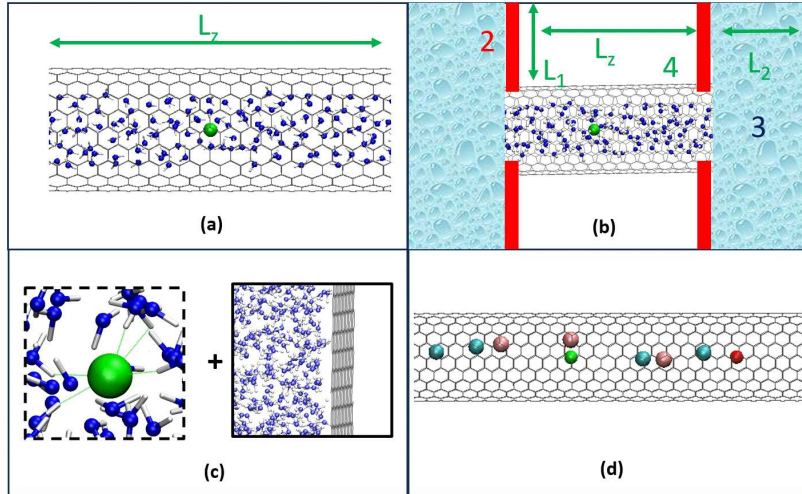


FIG. 1: Different contributions to $\Delta\Delta G_{hyd}$ in CNT's. (a) Intrinsic confinement effects, the focus of this work. (b) Reservoir interface potential (red); screening from reservoir (blue); and finite size effects (L_1 , L_2 , L_z , green) which are eliminated by the choice of our models. The numbers correspond to the text. (c) Reference system with infinite tube curvature. (d) Ion screening effect. Blue, white, gray, red, green, cyan, and pink represent O, H, C, Na, Cl, K, and Br atoms, respectively. Water is omitted from panel (d).

middle of these one-dimensional pores is unambiguous because the summed Coulomb interaction converges absolutely in isolated nanotubes, providing a confinement benchmark for Eqs. 1-2. Boundary contributions (Fig. 1b) can be calculated and then added separately. Although molecular modeling of electrolytes under cylindrical confinement has a long history,⁴⁰ to our knowledge $\Delta\Delta G_{hyd}$'s for individual ions have yet to be elucidated except in very narrow pores that disrupt the first hydration shells.⁴¹

We will also show that adding a background 1.0 M electrolyte (henceforth “ions”) strongly reduces $\Delta\Delta G_{hyd}$ in narrow nanotubes. This effect is not included in all modeling codes;⁴² some widely used implicit solvent methods also use as input the pure solvent isotropic ϵ but not the ionic strength.⁴³ ~ 1.0 M ion concentrations are relevant to sea water desalination,¹⁷ energy,^{19,20} and nanopore applications (e.g., membrane-based rejection of ions⁴) which exhibit regions with high local ion concentrations.

We omit reservoirs and extrapolate the length of the single wall CNT to infinity in order to pinpoint intrinsic confinement effects. The carbon-center-to-carbon-center radii chosen

are $R=7.5 \text{ \AA}$ and 12.5 \AA , which are similar to those of imogolite nanotubes.³⁹ We will show that these systems already generate significant ion confinement effects; more extreme environments like sub-nanometer diameter CNT's^{28,41} or sub-nanometer slits^{5,12} are not needed. We apply thermodynamic integration (TI) to the electrostatic contributions via MD simulations,

$$\Delta G_{\text{hyd}} = \int_0^1 d\lambda \langle dH(\lambda)/d\lambda \rangle_{\lambda}. \quad (3)$$

Here $\langle \rangle_{\lambda}$ represents thermal averaging in simulation cells with a partially charged $\text{Na}^{\lambda+}$ or $\text{Cl}^{\lambda-}$ ion frozen on the CNT axis. This is the cylindrical confinement version of single ion studies in unconfined liquid water.⁴⁴⁻⁴⁶ Our CNT models are not polarizable or metallic, which would bestow different dielectric behavior.^{25,47-50} The free energy of the same ion outside the tube is subtracted from Eq. 3. This eliminates the monopole term⁵¹ in simulation cells with net charges. In fact, ΔG_{hyd} can be calculated in different ways with different corrections,^{44,52} and they generally agree to $\sim 0.5 \text{ kcal/mol}$; see the Supporting Information (SI) document which also describes the statistical uncertainties and non-electrostatic contributions. To obtain $\Delta\Delta G_{\text{hyd}}$ requires a reference state; here it is a single ion removed from the liquid to infinity in vacuum, through a confining graphene wall with vanishing curvature (Fig. 1c) instead of the water-vapor interface in other applications.³⁷ This leads to a 8.9 kcal/mol shift favoring cations and disfavoring anions for the force fields used.

Figure 2a-b demonstrates that, in a $R=7.5 \text{ \AA}$ radius CNT, $\Delta\Delta G_{\text{hyd}}$ values in confined water are substantial ($3.7\text{-}7.8 \text{ kcal/mol}$) compared to $k_{\text{B}}T$. These effects, which should be readily detected in experiments, are highly asymmetric with respect to cation/anion exchange. $\Delta\Delta G_{\text{hyd}}$ for Cl^- decreases from 7.8 kcal/mol to 4.8 kcal/mol as R increases from 7.5 \AA to 12.5 \AA . In contrast, $\Delta\Delta G_{\text{hyd}}$ for Na^+ only drops from 3.7 to 3.0 kcal/mol .

The ΔG_{hyd} 's for confined ions used to calculate $\Delta\Delta G_{\text{hyd}}$ have been extrapolated to $L_z \rightarrow \infty$ (Fig. 2c-d). The ΔG_{hyd} differences between $L_z=118 \text{ \AA}$ and $L_z \rightarrow \infty$ are $5.4, 4.7, 5.3,$ and 5.2 kcal/mol for Na^+ at $R=7.5 \text{ \AA}$ and $R=12.5 \text{ \AA}$, and Cl^- in the two CNT's, respectively. The scaling/convergence behavior in Fig. 2c-d involves Ewald sums and is not directly measurable. In the SI, we apply real-space summation of a lattice model which is more relevant to experimental ΔG_{hyd} as a function of pore length. We also predict a quasi- $(1/L_z)$ scaling regime there, and estimate that a $L_z=30 \text{ \AA}$ tube model³⁴ overestimates the monovalent ion $\Delta\Delta G_{\text{hyd}}$ by $\sim 3 \text{ kcal/mol}$ compared to $L_z \rightarrow \infty$. This long-range requirement may impact the fitting of machine learning force fields, and may require explicit Coulomb

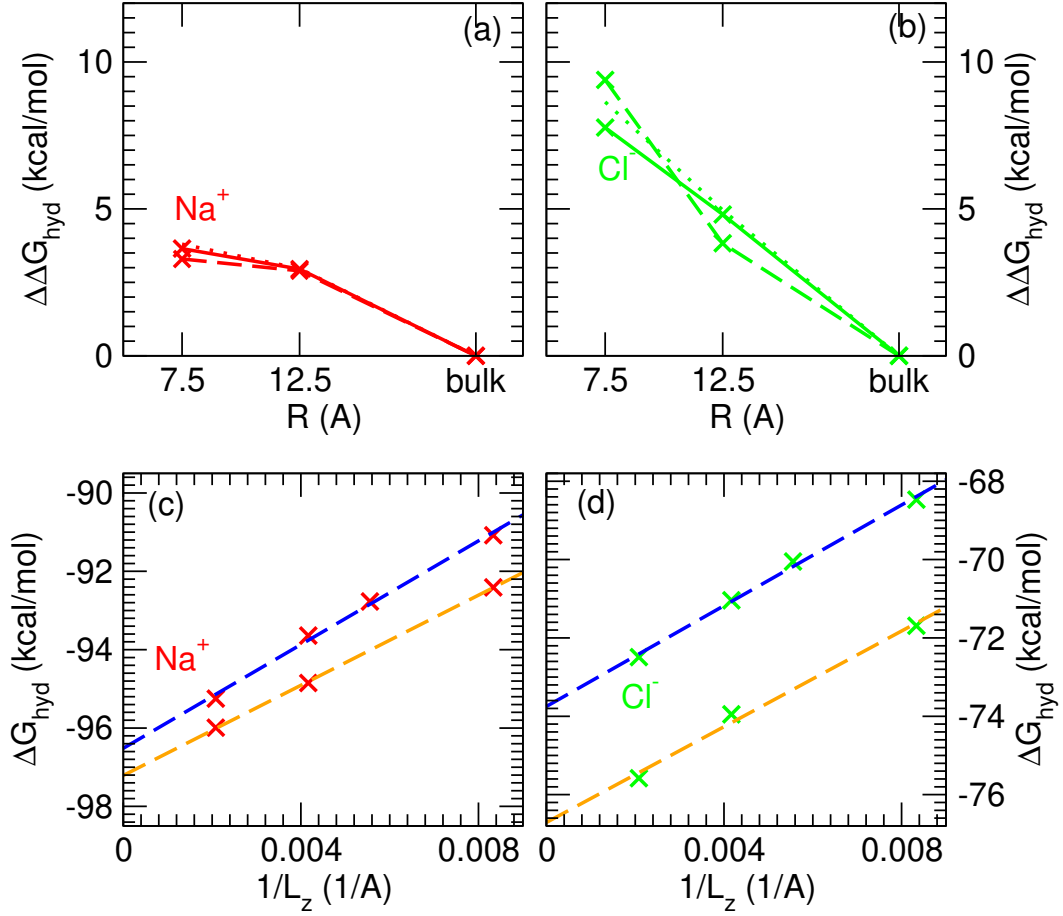


FIG. 2: (a)-(b) $\Delta\Delta G_{\text{hyd}}$ for Na^+ (red) and Cl^- (green) at different R , respectively, highlighting the anomalously large $\Delta\Delta G_{\text{hyd}}$ for Cl^- at $R=7.5$ Å. Dashed line: electrostatic contribution only; solid: total; dotted: total minus Lennard-Jones interaction with CNT. (c)-(d) Extrapolation of ΔG_{hyd} to infinite pore length for Na^+ and Cl^- , respectively. $R=7.5$ Å and $R=12.5$ Å are in blue and orange.

forces be introduced.^{5,53,54}

Next we allow sampling of ion positions in the x - y plane away from the CNT axis. The resulting radial ion distributions ($\rho_{\text{ion}}(r)$) depicted in Fig. 3a-b show that Cl^- is monotonically more favored at the pore axis at $R=7.5$ Å while Na^+ prefers regions where the local water density is lowest. Hence the large $\Delta\Delta G_{\text{hyd}}$ for Cl^- in the $R=7.5$ Å CNT is not due to lowered Cl^- probability at the pore center compared to Na^+ . Converting $\rho_{\text{ion}}(r)$ to Boltzmann weights relative to $\rho_{\text{ion}}(r=0)$ and integrating over r yield ΔG_{hyd} configuration corrections of +0.51 and +1.27 kcal/mol for Na^+ and Cl^- at $R=7.5$ Å, and +0.84 and +0.53 kcal/mol

at $R=12.5$ Å, respectively, after assuming tube volumes are given by the number of H_2O present multiplied by a molecular volume of 29.9 Å³. These corrections are a small fraction of the $\Delta\Delta G_{\text{hyd}}$ reported above; they would have made the Na^+/Cl^- asymmetry in the $R=7.5$ Å CNT even larger. Here we omit them because they would add non-intrinsic confinement effects (e.g., close-proximity ion interactions with CNT interior surfaces) to the $\Delta\Delta G_{\text{hyd}}$'s. This point highlights the need to have models with $\Delta\Delta G_{\text{hyd}} > 1$ kcal/mol for proof-of-principle studies to overcome computational uncertainties.

The $R=7.5$ Å behavior (Fig. 3a) is in best agreement with the 1.15 nm diameter CNT results for Na^+ and Cl^- in Ref. 55. This is because, in our work, R is measured from the center of one CNT carbon atom to another without subtracting the diameter of carbon atoms. The force fields used are also different from those in Ref. 55.

$\Delta\Delta G_{\text{hyd}}$ is predicted to be smaller for Na^+ than the larger Cl^- . This contradicts the canonical Born Equation. The ionic radii of Na^+ and Cl^- are often quoted as 0.95 Å and 1.81 Å. Even if one fits to the unconfined ΔG_{hyd} without the boundary term (Fig. 1c), the Na^+ and Cl^- a_{eff} would at best be similar (1.84 and 1.83 Å). According to Eq. 2, if $\epsilon=13.3$ in the $R=7.5$ Å CNT,³³ $\Delta\Delta G_{\text{hyd:B}}$ for Na^+ and Cl^- would be 5.6 and 5.7 kcal/mol respectively with these a_{eff} instead of 3.7 and 7.8 kcal/mol.

Next we compute the restricted Madelung potential, $\phi_{\text{M}}(r)$, to examine the origin of the Na^+/Cl^- asymmetry.

$$\phi_{\text{M}}(r) = \langle c_{\text{M}} \sum_i^l q_i / (\epsilon_w |\mathbf{r}_a - \mathbf{r}_i|) \rangle. \quad (4)$$

Here \mathbf{r}_a is the position of the $\text{Na}^{\lambda+}$ or $\text{Cl}^{\lambda-}$, the sum is over point charges q_i of the classical force field model with minimum image convention and molecular cut-off subject to the constraint that the distance between the oxygen site of the H_2O being summed and the ion is less than r , atomic units are used, and $c_{\text{M}} = \pm\lambda$ for $\text{Na}^{\lambda+}/\text{Cl}^{\lambda-}$ to make $\phi_{\text{M}}(r)$ negative definite.

Figs. 3c-d, depicted for $\lambda=1$, show that the magnitudes of the $\phi_{\text{M}}(r)$'s for Cl^- at $r < 3.85$ Å and $r < 6.20$ Å are in fact larger (more favorable) for the $R=7.5$ Å CNT than $R=12.5$ Å. Results for other λ values are qualitatively similar. This shows, counter-intuitively, that the anomalously large Cl^- $\Delta\Delta G_{\text{hyd}}$ at $R=7.5$ Å does not arise from short-range interactions. By elimination, it must be due to competition among long-range effects: (1) dielectric solvation (agnostic to the sign of the charge); (2) the interactions with preferentially oriented water at the CNT interior surface causing the 8.9 kcal/mol interfacial potential favoring cations; and

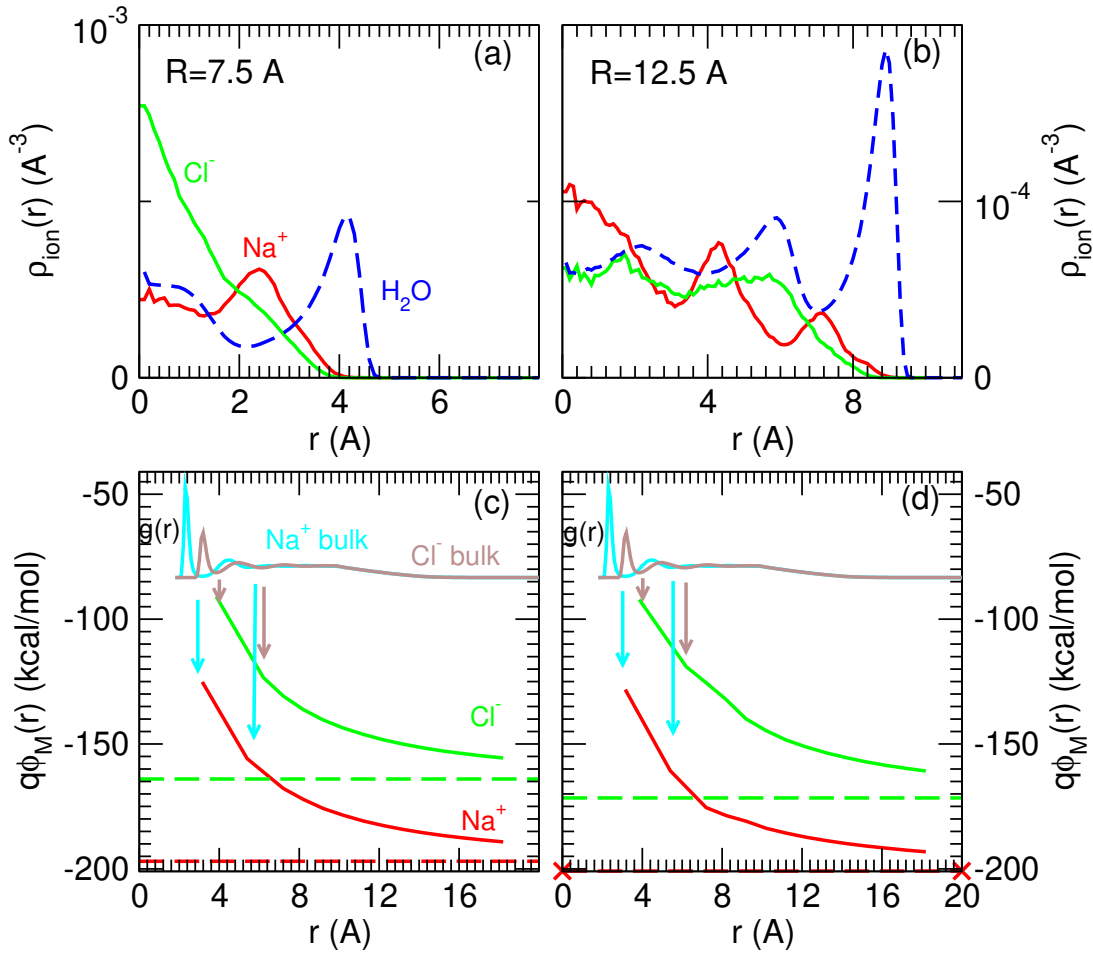


FIG. 3: (a)-(b) Radial distribution of Na^+/Cl^- for $R=7.5 \text{ \AA}$ and $R=12.5 \text{ \AA}$, respectively. Each cell contains either a Na^+ (red) or a Cl^- (green). $L_z=118 \text{ \AA}$. Water density profiles (blue) are scaled by $1/200$ and $1/500$ in the two panels, respectively. (c)-(d) Madelung potential at $R=7.5 \text{ \AA}$ and $R=12.5 \text{ \AA}$, respectively, delimited by molecular cut-offs (r). Red/blue denote values for confined Na^+/Cl^- . Dashed lines are $\phi_M(r)$ with $r \rightarrow \infty$. The $g(r)$'s of bulk water with the ions are also depicted as guides.

(3) CNT curvature which modifies this interfacial potential. Asymmetry between cations and anions has also been noted for contact ion pairs in slit pores⁵⁶ and other contexts.⁵⁷

Finally, we add a 1.0 M KBr background electrolyte in the $R=7.5 \text{ \AA}$ CNT. Wider CNT's exhibit smaller confinement effects in 1.0 KBr,³³ and are not considered. Once again we use the Born formula (Eq. 1) as starting point. It has often been reported that the water dielectric constant ϵ_w is reduced in the presence of ions.⁵⁸ If adding ions reduces ϵ_w and ϵ under confinement proportionally, $\Delta\Delta G_{\text{hyd}}$ should increase. However, such decreased ϵ_w

and ϵ are calculated/measured at MHz/GHz frequencies, while ion hydration corresponds to zero frequency at which ϵ of the medium diverges for electrolytes.³¹ In our recent MD simulations, a 0.5 M background electrolyte appears to eliminate the $\Delta\Delta G_{\text{hyd}}$ predicted in water confined in a nanoslit.³⁶ We will show that adding 1.0 M KBr also decreases $\Delta\Delta G_{\text{hyd}}$ here, qualitatively consistent with setting $\epsilon=\infty$ in Eq. 1.

Our approach used for pure water needs to be modified for electrolytes. To illustrate this, consider the single-ion TI ΔG_{hyd} in Fig. 4a-b which correspond to 1.0 M KBr electrolytes in the $L_z=118$ Å cell. If the numbers of K^+ and Br^- are equal, and the cell is charge-neutral at $\lambda=0$ during TI (but not at any other λ , Eq. 3), the single-ion ΔG_{hyd} 's are almost the same at 0.0 M or 1.0 M KBr for the confined Na^+ (Fig. 3a) and the confined Cl^- (Fig. 3b). If the cell has one less K^+ or Br^- and is charge-neutral at $\lambda=1$, the sum of single-ion ΔG_{hyd} becomes ~ 21.2 kcal/mol more favorable. In contrast, in unconfined electrolytes, whether the numbers of K^+ and Br^- are equal or not only has a ~ 1 kcal/mol effect on ΔG_{hyd} . The reason is that the canonical ensemble we use suppresses charge fluctuations,⁵⁹ which is particularly significant if the net charge is concentrated inside the CNT, not smeared across the entire cell. In principle, Grand Canonical Monte Carlo (GCMC) can be used to remove this ambiguity. GCMC can add counter-ions and make the simulation cell probabilistically charge-neutral, but this adds a significant computational cost.⁶⁰

To circumvent this ambiguity, we place a $\text{Na}^{\lambda+}$ and a $\text{Cl}^{\lambda-}$ ion on the CNT axis either at contact ($z_c=2.75$ Å apart) or $z_f = L_z/2$ apart from each other at 1.0 M KBr concentration, and simultaneously charge both ions to $\lambda=\pm 1$ using TI. Now the system is charge-neutral over the entire λ -path.

The resulting contact-ion-pair $\Delta\Delta G_{\text{pair}}(z_c)$ are first calculated in confined water and confined 1.0 M KBr (Fig. 4c). They are within 0.3-1.4 kcal/mol of the unconfined $\Delta\Delta G_{\text{hyd}}$ for Na^+ and Cl^- combined. To a first approximation, these uncharged contact ion pairs (CIP's) do not incur monopole confinement penalties (Eqs. 1-2).

In 1.0 M KBr, the confinement penalties for well-separated Na^+/Cl^- are drastically reduced from those in water, taken as sum of Na^+ and Cl^- contributions from Fig. 2c-d (Fig. 4c). They are also less L_z -dependent. When the Na^+ and Cl^- are separated by $z=28$ Å at $L_z=472$ Å (Fig. 4c), $\Delta\Delta G_{\text{pair}}(z)$ is already comparable to that at $z=L_z/2$. Even though our ion pair approach cannot separate the Na^+ and Cl^- contributions, the results strongly suggest that $\Delta\Delta G_{\text{hyd}}$ for both ions are much reduced. We have further repeated the calcu-

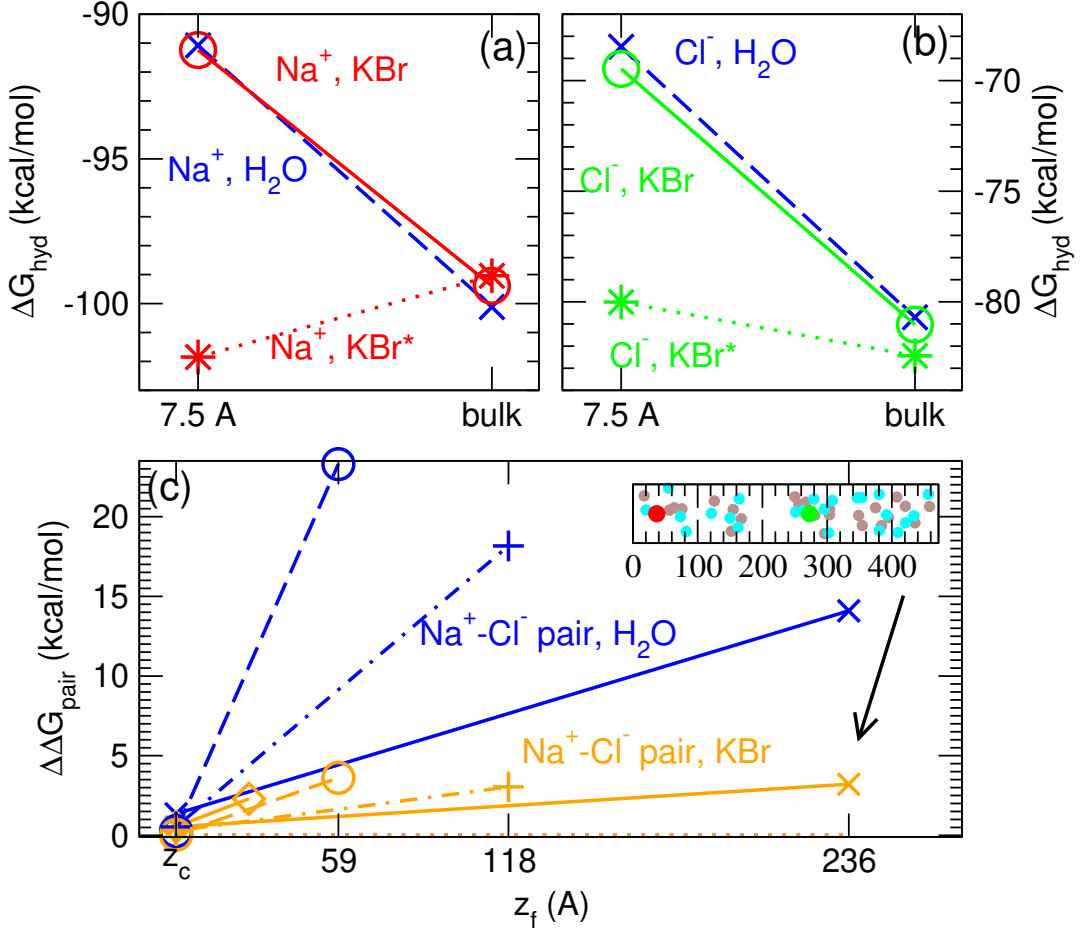


FIG. 4: (a)-(b): ΔG_{hyd} for isolated Na^+ and Cl^- , respectively, in the $R=7.5 \text{ \AA}$ CNT. Blue/crosses: in water. Solid red or green with circles: in 1.0 M KBr with equal number of cations and anions. Dotted red or green with stars: in 1.0 M KBr with one less cation or anion. $L_z=118 \text{ \AA}$. These panels show that single-ion calculations are ambiguous at finite ion concentrations. (c) $\Delta\Delta G_{\text{pair}}(z)$ for $\text{Na}^+\text{-Cl}^-$ ion pair in contact ($z=z_c$) or half a box length away ($z=z_f=L_z/2$) in 1.0 M KBr (orange), and sum of ΔG_{hyd} for isolated Na^+ plus Cl^- in water (blue, from Fig. 2c-d). Solid/cross, dot-dashed/plus, and dashed/circle are for $L_z=472 \text{ \AA}$, $L_z=236 \text{ \AA}$, and $L_z=118 \text{ \AA}$. The diamond is for $L_z=472 \text{ \AA}$, $z=28 \text{ \AA}$. Inset: ion segregation in one MD snapshot. Red, green, brown, and cyan are Na^+ , Cl^- , K^+ , and Br^- .

lations in the $L_z=472 \text{ \AA}$ simulation cell at a lower, 0.5 M KBr concentration; $\Delta\Delta G_{\text{pair}}(z_f)$ is very similar (lower by 0.21 kcal/mol) compared with the 1.0 M KBr simulation.

In other words, the KBr ions *screen* most of the water- Na^+/Cl^- interactions that lead to the confinement penalty. This behavior can be anticipated from and reconciled with previous

predictions of background ions drastically reducing the free energy cost of pulling apart contact ion pairs inside this CNT.³³ In solid state materials, all mobile charges are recognized to screen all other charges. In unconfined liquids, the role ions play in screening is sometimes omitted.^{42,43} At low ion concentrations, the ion screening contribution can be estimated using the Debye-Hückel (DH) approach.⁶¹⁻⁶⁴ The correction to ΔG_{hyd} is $-q^2/[2\epsilon r_D(1 + a_{\text{eff}}/r_D)]$ in atomic units in unconfined electrolytes, where r_D is the Debye screening length⁶¹⁻⁶³ and $q=\pm 1$ is the ionic charge. As $r_D \propto \epsilon^{0.5}$, this attractive ion-ion interaction $\propto 1/\epsilon^{1.5}$; other formulations exhibit more complex, cross-over scaling behavior.⁶⁵ Using $a_{\text{eff}}=1.84 \text{ \AA}$ (which is force field-dependent) and taking $\epsilon=60$ for an unconfined 1.0 M monovalent electrolyte,⁵⁸ the DH approach yields a correction of -1.2 kcal/mol for $\text{Na}^+ + \text{Cl}^-$. In contrast, in our $L_z=472 \text{ \AA}$, $R=7.5 \text{ \AA}$ cell, the 1.0 KBr reduces $\Delta\Delta G_{\text{pair}}$ by 8.2 to 9.1 kcal/mol depending on whether the Na^+ and Cl^- are placed 236 or 28 \AA apart – almost an order of magnitude larger. This suggests that more quantitative solvation theories^{42,66} than DH need to be developed to quantify confinement in electrolytes, particularly because both ϵ and r_D may be anisotropic in nanopores. This finding may also be relevant to unconfined battery electrolytes with low solvent ϵ 's.^{67,68}

In the largest ($L_z=472 \text{ \AA}$) cell, KBr aggregation behavior is observed; gaps without ions appear. Furthermore, the 1.0 M KBr drastically decreases the favorable ion-pairing free energy among the K^+ and Br^- themselves, and decreases the persistence times of K-Br CIP's. See the SI for details. Nevertheless, more K^+/Br^- CIP's (50%) are formed inside the $R=7.5 \text{ \AA}$ CNT than in the unconfined electrolyte (33%), likely due to the residual confinement effect in 1.0 KBr (Fig. 4c). For a quantitative comparison with ion-pairing experiments,⁹ lower electrolyte concentrations, multivalent ions, the dielectric materials outside the CNT, charges on nanopore surfaces, more accurate force fields, and CNT polarizability need to be considered. We defer those to future work.

In conclusion, we have calculated the intrinsic confinement free energy penalties ($\Delta\Delta G_{\text{hyd}}$) of single ions in water-filled non-polarizable CNT's. In a $R=7.5 \text{ \AA}$ CNT, $\Delta\Delta G_{\text{hyd}} \sim 3.7$ and 7.8 kcal/mol for Na^+ and Cl^- , respectively. Na^+ is strongly favored over Cl^- in this CNT, contrary to what the canonical Born Equation²¹ would predict, suggesting the Born formulation needs to be modified for strongly confined media. $\Delta\Delta G_{\text{hyd}}$ converges slowly with CNT length (L_z), depending on the computational method used; at $L_z=472 \text{ \AA}$, it is within 1 kcal/mol of the value extrapolated to infinity. By considering a

Na^+/Cl^- pair far apart along the CNT axis, we show that adding 1.0 M KBr significantly reduces $\Delta\Delta G_{\text{hyd}}$. This emphasizes that ions strongly screen water-ion interactions, of which $\Delta\Delta G_{\text{hyd}}$ in confined water is one manifestation. Inferring ion solvation properties from the dielectric properties of pure, confined water alone²²⁻³³ would omit this crucial contribution. We identify finite-concentration ion-screening as a major, unheralded consequence of confined electrolytes in cylindrical nanopores.

Supporting Information Available

The Supporting Information is available free of charge at <https://pubs.acs.org/>. Discussion of computational details; convergence tests; supplemental results; lattice model real space summation.

Acknowledgement

We thank Dusan Bratko, Marialore Sulpizi, Jeff Greathouse, Ward Thompson, Anastasia Ilgen, and Tuan Ho for valuable suggestions. This work is based on materials support by the U.S. DOE Office of Basic Energy Sciences, Division of Chemical Sciences, Geosciences, and Biosciences under Field Work Proposal Number 24-015452 at Sandia National Laboratories. This article has been authored by an employee of National Technology & Engineering Solutions of Sandia, LLC under Contract No. DE-NA0003525 with the U.S. Department of Energy (DOE). The employee owns all right, title and interest in and to the article and is solely responsible for its contents. The United States Government retains and the publisher, by accepting the article for publication, acknowledges that the United States Government retains a non-exclusive, paid-up, irrevocable, world-wide license to publish or reproduce the published form of this article or allow others to do so, for United States Government purposes. The DOE will provide public access to these results of federally sponsored research in accordance with the DOE Public Access Plan <https://www.energy.gov/downloads/doe-public-access-plan>. This paper describes objective technical results and analysis. Any subjective views or opinions that might be expressed in the paper do not necessarily represent the views of the U.S. Department of Energy or the United States Government.

References

- ¹ Gonella, G.; Backus, E.H.G.; Nagata, Y.; Bonthuis, D.J.; Loche, P.; Schlaich, A.; Netz, R.R.; Kühnle, A.; McCrum, I.T.; Koper, M.T.M.; *et al.* Water at Charged Interfaces. *Nat. Chem.* **2021**, *5*, 466-485.
- ² Corti, H.R.; Appignanesi, G.A.; Barbosa, M.C.; Bordin, J.R.; Calero, C.; Camisasca, G.; Elola, M.D.; Franzese, G.; Gallo, P.; Hassanali, A.; *et al.* Structure and Dynamics of Nanoconfined Water and Aqueous Solutions. *Eur. Phys. J. E* **2021**, *44*, 136.
- ³ Ilgen, A.G.; Leung, K.; Criscenti, L.J.; Greathouse, J.A. Adsorption at Nanoconfined Solid-Water Interfaces. *Annu. Rev. Phys. Chem.* **2023**, *74*, 169-191.
- ⁴ Epsztein, R.; DuChanois, R.M.; Ritt, C.L.; Noy, A.; Elimelech, M. Towards Single-Species Selectivity of Membranes with Subnanometre Pores. *Nat. Nanotech.* **2020**, *15*, 426-436.
- ⁵ Fong, K.D.; Sumic, B.; O'Neill, N.; Schran, C.; Grey, C.P.; Michaelides, A. The Interplay of Solvation and Polarization Effects on Ion Pairing in Nanoconfined Electrolytes. *Nano Lett.* **2024**, *24*, 5024-5030.
- ⁶ Litman, Y.; Chiang, K.-Y.; Seki, T.; Nagata, Y.; Bonn, M. Surface Stratification Determines the Interfacial Water Structure of Simple Electrolyte Solutions. *Nat. Commun.* **2024**, *16*, 644-650.
- ⁷ Munoz-Santiburcio, D.; Marx, D. Confinement-Controlled Aqueous Chemistry Within Nanometric Slit Pores. *Chem. Rev.* **2021**, *121*, 6293-6320.
- ⁸ Ilgen, A.G.; Kabengi, N.; Smith, J.G.; and Sanchez, K.M.M. Ion Solvation as a Predictor of Lanthanide Adsorption Structures and Energetics in Alumina Nanopores. *Commun. Chem.* **2023**, *6*, 172.
- ⁹ Sit, I.; Fashina, B.T.; Baldo, A.P.; Leung, K.; Grassian, V.H.; Ilgen, A.G. Formic and Acetic Acid pKa Values Increase Under Nanoconfinement. *RSC Adv.* **2023**, *13*, 23147-23157.
- ¹⁰ Fashina, B.T.; Ilgen, A.G. Lanthanide Adsorption Kinetics in Silica Nanopores. **2026**, *400*, 113906.
- ¹¹ Dasgupta, S.; Saha, S.; Paesani, F. Reactivity of Nanoconfined Water is Modulated by the Properties of Confining Materials. *J. Phys. Chem. Lett.* **2025**, *16*, 11996-12004.
- ¹² Dasgupta, S.; Saha, S.; Paesani, F. Sub-nanometer Confinement Suppresses Autoionization of Water. *J. Am. Chem. Soc.* **2025**, *147*, 25167-25173.

- ¹³ Wang, Y.; Zhu, Y.; Zuo, X.B.; He, L.L.; Jun, Y.S. Soft Nanoconfinement Nucleates and Stabilizes Ultrasmall Amorphous Calcium Carbonate from Aggregation. *Cryst. Growth & Design* **2025**, *25*, 8325-8331.
- ¹⁴ Luo, T.; Abdu, S.; Wessling, M. Selectivity of Ion Exchange Membranes: A Review. *J. Memb. Sci.* **2018**, *555*, 429-454.
- ¹⁵ Mukherjee, P.; Sengupta, A.K. Ion Exchange Selectivity as a Surrogate Indicator of Relative Permeability of Ions in Reverse Osmosis Processes. *Environ. Sci. Tech.* **2003**, *37*, 1432-1440.
- ¹⁶ Freger, V. Dielectric Exclusion, an Eminence Grise. *Adv. Coll. Interface Sci.* **2023**, *319*, 102972.
- ¹⁷ Elimelech, M.; Phillip, W.A. The Future of Seawater Desalination: Energy, Technology, and the Environment. *Science*, **2011**, *333*, 712-717.
- ¹⁸ Wild, B.; White, C.E.; Bourg, I.C. Molecular Dynamics Simulations of Reverse Osmosis in Silica Nanopores. *J. Phys. Chem. C* **2022**, *126* 9167-9172.
- ¹⁹ Farber, E.M.; Seraphim, N.M.; Tamakuwala, K.; Stein, A.; Rücker, M.; Eisenberg, D. Porous Materials: The Next Frontier in Energy Technologies. *Science* **2025**, *390*, eadn9391.
- ²⁰ Jeanmairat, G.; Rotenberg, B.; Borgis, D.; Salanne, M. Study of Water-Graphene Capacitor with Molecular Density Functional Theory. *J. Chem. Phys.* **2019**, *151*, 124111.
- ²¹ Born, M. Volumen und Hydratationswärme der Ionen. *Z. Phys.* **1920**, *1*, 45-48.
- ²² Fumagalli, L.; Esfandiar, A.; Fabregas, R.; Hu, S.; Ares, P.; Janardanan, A.; Yang, Q.; Radha, B.; Taniguchi, T.; Watanabe, K.; *et al.* Anomalously Low Dielectric Constant of Confined Water. *Science* **2018**, *360*, 1339-1342.
- ²³ Olivieri, J.-F.; Hynes, J.T.; Laage, D. Confined Water's Dielectric Constant Reduction is Due to the Surrounding Low Dielectric Media and Not to Interfacial Molecular Ordering. *J. Phys. Chem. Lett.* **2021**, *12*, 4319-4326.
- ²⁴ Schaaf, C.; Gekle, S. Spatially Resolved Dielectric Constant of Confined Water and Its Connection to the Non-Local Nature of Bulk Water. *J. Chem. Phys.* **2016**, *145*, 084901.
- ²⁵ Loche, P.; Ayaz, C.; Schlaich, A.; Uematsu, Y.; Netz, R.R. Giant Axial Dielectric Response in Water-Filled Nanotubes and Effective Electrostatic Ion-on Interactions from a Tensorial Dielectric Model. *J. Phys. Chem. B* **2019**, *123*, 10850-10857.
- ²⁶ Motevaselian, M.H.; Aluru, N.R. Universal Reduction in Dielectric Response of Confined Fluids. *ACS Nano* **2020**, *14*, 12761-12770.
- ²⁷ Motevaselian, M.H.; Aluru, N.R. Confinement-Induced Enhancement of Parallel Dielectric Per-

- mittivity: Super Permittivity Under Extreme Confinement. *J. Phys. Chem. Lett.* **2020**, *11*, 10532-10537.
- ²⁸ Andrade, M.F.C.; Aluru, N.R.; Pham, T.A. Nonlinear Effects of Hydrophobic Confinement on the Electronic Structure and Dielectric Response of Water. *J. Phys. Chem. Lett.* **2024**, *15*, 6872-6879.
- ²⁹ Mondal, S.; Bagchi, B. Water in Carbon Nanotubes: Pronounced Anisotropy in Dielectric Dispersion and its Microscopic Origin. *J. Phys. Chem. Lett.* **2019**, *10*, 6289-6292.
- ³⁰ Ghoufi, A.; Szymczyk, A.; Renou, R.; Ding, M. Calculation of Local Dielectric Permittivity of Confined Liquids from Spatial Dipolar Correlations. *EPL* **2012**, *99*, 37008.
- ³¹ Leung, K. Finding Infinities in Nanoconfined Geothermal Electrolyte Static Dielectric Properties and Implications on Ion Adsorption/Pairing. *Nano Lett.* **2023**, *23*, 8868-8874.
- ³² Underwood, T.R.; Bourg, I.C. Dielectric Properties of Water in Charged Nanopores. *J. Phys. Chem. B* **2022**, *126*, 2688-2698.
- ³³ Leung, K.; Ho, T.A. Beyond Dielectric Formulations: Local Descriptors of Electrolyte Properties in Cylindrical Nanopores. *J. Phys. Chem. C* **2025**, *129*, 12197-12203.
- ³⁴ Leung, K.; Rempe, S.B. Ion Rejection by Nanoporous Membranes in Pressure-Driven Molecular Dynamics Simulations. *J. Comp. Theor. Nanoscience* **2009**, *6*, 1948-1955.
- ³⁵ Ho, T.A. Influence of Ion Pairing on Ion and Counterion Retention in Neutral Nanopores of Gibbsite and Kaolinite. *Nanoscale*, **2025**, *17*, doi:10.1039/d5nr01746g.
- ³⁶ Baldo, A.P.; Ilgen, A.G.; Leung, K. Deprotonation of Formic, Acetic Acids and Bicarbonate Ion in Slit Silica Nanopores at Infinite Dilution and in the Presence of Electrolytes. *J. Coll. Interface Sci.* **2024**, *674*, 482-489.
- ³⁷ Wilson, M.A.; Pohorille, A.; Pratt, L.R. Comment on "Study on the Liquid-Vapor Interface of Water. I. Simulation Results of Thermodynamic Properties and Orientational Structure." *J. Chem. Phys.* **1989**, *90*, 5211.
- ³⁸ Leung, K. Surface Potential at the Air-Water Interface Computed Using Density Functional Theory. *J. Phys. Chem. Lett.* **2010**, *1*, 496-499.
- ³⁹ Gonzales, R.I.; Royas-Nunez, J.; Valencia, F.J.; Munoz, F.; Baltazar, S.E.; Allende, S.; Rogan, J.; Valdivia, J.A.; Kiwi, M.; Ramirez, R.; Greathouse, J.A. Imogolite in Water: Simulating the Effects of Nanotube Curvature on Structure and Dynamics. *Appl. Clay Sci.* **2020**, *191*, 105582.
- ⁴⁰ See, e.g., Vlachy, V.; Haymet, A.D.J. Electrolytes in Charged Micropores. *J. Am. Chem. Soc.*

- 1989, *111*, 477-481.
- ⁴¹ Neklyudov, V.; Freger, V. Ion Coupling, Bonding, and Transfer in Narrow Carbon Nanotubes. *Small*, **2024**, *20*, 2402327.
- ⁴² Ringe, S.; Hormann, N.G.; Oberhofer, H.; Reuter, K Implicit Solvation Methods for Catalysis at Electrified Interfaces. *Chem. Rev.* **2022**, *122*, 10777-10820.
- ⁴³ Scalmani, G.; Frisch, M.J. Continuous Surface Charge Polarizable Continuum Models of Solvation. I. General Formalism. *J. Chem. Phys.* **2010**, *132* 114110.
- ⁴⁴ Hummer, G.; Pratt, L.R.; Garcia, A.E. Free Energy of Ion Hydration. *J. Phys. Chem.* **1996**, *100*, 1206-1215.
- ⁴⁵ Hummer, G.; Pratt, L.R.; Garcia, A.E. Ion Sizes and Finite-size Corrections for Ion-Solvation Free Energies. *J. Chem. Phys.* **1997**, *107*, 9275-9277.
- ⁴⁶ Hofer, T.S.; Hünenberger, P.H. Absolute Proton Hydration Free Energy, Surface Potential of Water, and Redox Potential of Hydrogen Electrode from First Principles: QM/MM MD Free-Energy Simulations of Sodium and Potassium Hydration. *J. Chem. Phys.* **2018**, *148*, 222814.
- ⁴⁷ A.A. Kornyshev, A.I. Rubinshtein, and M.A. Vorotyntsev, Image Potential Near a Dielectric-Plasma-Like Medium Interface. *Phys. Stat. Sol. (B)* **84**, 125 (1977).
- ⁴⁸ C.C. Rochester, A.A. Lee, G. Pruessner, and A.A. Kornyshev, Interionic Interactions in Conducting Nanoconfinement. *ChemPhysChem* **14**, 4121 (2013).
- ⁴⁹ Jimenez-Angeles, F.; Ehlen, A.; Olvera de la Cruz, M. Surface Polarization Enhances Ionic Transport and Correlations in Electrolyte Solutions Nanoconfined by Conductors. *Faraday Discuss.* **2023**, *246*, 576-591.
- ⁵⁰ Kistwal, T.; Kanhaiya, K.; Buchmann, A.; Ma, C.; Nikolic, J.; Ackermann, J.; Galonska, P.; Nalige, S.S.; Havenith, M.; Sulpizi, M.; Kruss, S. Light-induced Quantum Friction of Carbon Nanotubes in Water. <http://arxiv.org/abs/2503.12580>.
- ⁵¹ Makov, G.; Payne, M.C. Periodic Boundary Conditions in *Ab Initio* Calculations, *Phys. Rev. B* **1994**, *51*, 4014-4022.
- ⁵² Adriaanse, C.; Cheng, J.; Chau, V.; Sulpizi, M.; VandeVondele, J.; Sprik, M. Aqueous Redox Chemistry and the Electronic Band Structure of Liquid Water. *J. Phys. Chem. Lett.* **2012**, *3*, 3411-3415.
- ⁵³ Zhu, J.-X.; Cheng, J. Machine Learning Potential for Electrochemical Interfaces with Hybrid Representation of Dielectric Response. *Phys. Rev. Lett.* **2025**, *135*, 018003.

- ⁵⁴ Cai, K.; Zhang, C.; Wu, X. Simulations of Dielectric Permittivity of Water by Machine Learned Potentials with Long-range Coulombic Interactions. *J. Chem. Phys.* **2025**, *163*, 184503.
- ⁵⁵ Xu, M.; Qiu, H., Shen, C.; Zhang, Z.; Guo, W. Ion Hydration under Nanoscale Confinement: Dimensionality and Scale Effects. *J. Phys. Chem. Lett.* **2022**, *13*, 4815-4822.
- ⁵⁶ Jimenez-Angeles, F.; Harmon, K.J.; Nguyen, T.D.; Fenter, P.; and Olvera de la Cruz, M. Nonreciprocal Interactions Induced by Water in Confinement. *Phys. Rev. Res.* **2020**, *2*, 043244.
- ⁵⁷ Dhakal, D.; Driscoll, D.M. Govind, N.; Stack, A.G.; Rampal, N.; Schenter, G.; Mundy, C.J.; Fister, T.T.; Fulton, J.L.; Balasubramanian, M.; Seidler, G.T. The Evolution of Solvation Symmetry and Composition in Zn Halide Aqueous Solutions from Dilute to Extreme Concentrations. *Phys. Chem. Chem. Phys.* **2023**, *25*, 22650-22661.
- ⁵⁸ See, e.g., Zhang, C.; Yue, S.; Panagiotopoulos, A.Z.; Klein, M.L.; Wu, X. Why Dissolving Salt in Water Decreases Its Dielectric Permittivity. *Phys. Rev. Lett.* **2023**, *131*, 076801.
- ⁵⁹ Svensson, Bo R.; Woodward, C.E. Widom's Method for Uniform and Non-Uniform Electrolyte Solutions. *Mol. Phys.* **1988**, *64*, 247-259.
- ⁶⁰ Moucka, F.; Bratko, D.; Luzar, A. Electrolyte Pore/Solution Partitioning by Expanded Grand Canonical Ensemble Monte Carlo Simulation. *J. Chem. Phys.* **2015**, *142*, 124705.
- ⁶¹ Van der Lubbe, S.C.C.; Canepa, P. Modeling the Effects of Salt Concentration on Aqueous and Organic Electrolytes. *NPJ Comput. Mater.* **2023**, *9*, 175.
- ⁶² Henriksen, N.E. On the Rate Constant for Reactions Between Ions in Solution: A Simple Unification of the Born and Debye-Hückel Models. *Phys. Chem. Chem. Phys.* **2025**, *27*, 1752-1755.
- ⁶³ Valisko, M.; Boda, D. Resurrection of Hückel's Idea: Decoupling Ion-Ion and Ion-Water Terms in Activity Coefficients via the State-Dependent Dielectric Constant. *Fluid Phase Equil.* **2023**, *572*, 113826.
- ⁶⁴ See also, for Poisson-Boltzmann-like corrections, dos Santos, A.P.; Uematsu, Y.; Rathert, A.; Loche, P.; Netz, R.R. Consistent Description of Ion-Specificity in Bulk and at Interfaces by Solvent Implicit Simulations and Mean-Field Theory. *J. Chem. Phys.*, **2020**, *153*, 034103.
- ⁶⁵ Gillespie, D.; Valisko, M.; Boda, D. Electrostatic Correlations in Electrolytes: Contribution of Screening Ion Interactions to the Excess Chemical Potential. *J. Chem. Phys.* **2021**, *155*, 221102.
- ⁶⁶ Duignan, T.T.; Baer, M.D.; Mundy, C.J. Ions Interacting in Solution: Moving from Intrinsic to Collective Properties. **2016**, *23*, 58-65.

- ⁶⁷ Pastel, G.R.; Pollard, T.P.; Borodin, O.; Schroeder, M.A. From Ab Initio to Instrumentation: A Field Guide to Characterizing Multivalent Liquid Electrolytes. *Chem. Rev.* **2025**, *125*, 3059-3164.
- ⁶⁸ Skiba, D.A.; Melemed, A.M.; Gallant, B.M. Experimental Pathways for Unlocking Thermodynamics of Ion Coordination in Battery Electrolytes. *J. Phys. Chem. C* **2026**, *130*, 3-17.